Supplementary Information for: Helical Electronic Transitions of Spiroconjugated Molecules

Marc H. Garner and Clemence Corminboeuf

Laboratory for Computational Molecular Design, Institute of Chemical Sciences and Engineering, Ecole Polytechnique federale de Lausanne (EPFL), 1015 Lausanne, Switzerland; E-mail: clemence.corminboeuf@epfl.ch

Table of Contents

A. Computational Details

All molecular structures were optimized in their electronic ground state at the ωB97X-D[1]/def2-TZVP[2] level using the Gaussian program package.[3] Structural optimizations were completed according to the *tight* criteria. Integrals were evaluated on the *ultrafine* grid. Frequency analysis was done to ensure that all molecules have been optimized to local energy minima. All optimized structures are included as supporting files in xyz format. Molecular orbitals (MOs) and electron densities were rendered using Avogadro. MO were visualized with iso-value = 0.02, and densities with iso-value = 0.002 unless otherwise noted.[4-5] Atomic orbitals were visualized using wxMacMolPlt.[6] Excited-state computations were carried out using linear response time-dependent (TD) density functional theory (DFT) at the ωB97X-D[1]/def2-TZVP[2] level as implemented in the Gaussian program package.[3] While the excited state energies are not influenced by the dispersion correction, the ωB97X-D variant is known to be highly robust.[7] Chiroptical properties were assessed using this method; for more detail on the approach for computing molecular optical activity we refer to the extensive reviews by Autschbach.[8-9] All rotatory strengths reported were computed with velocity gauge representation. Conformation-resolved UV-Vis and electronic circular dichroism (ECD) spectra were generated using Gaussview by assuming a gaussian line-shape with the default parameter for the standard deviation, σ=1/3099.6 nm^{-1}.[10]

Details for the electronic transitions of allene, 1,3-dimethylallene, spiropentadiene, and 1,4-dimethylspiropentadiene are listed in Table S1-S4. Note that for D_{2d}-symmetry spiropentadiene the configuration interaction coefficients of the E transitions are meaningless due to the degeneracy of the transitions.

Table S1. $\pi \rightarrow \pi^*$ transitions of allene

Transition	Configuration	E (eV)	Oscillator strength
$S_0 \rightarrow S_4$	$0.49\cdot(\pi_y \rightarrow \pi_y^*) - 0.49\cdot(\pi_x \rightarrow \pi_x^*)$	8.12	1.19
$S_0 \rightarrow S_3$	$0.50\cdot(\pi_y \rightarrow \pi_y^*) + 0.50\cdot(\pi_x \rightarrow \pi_x^*)$	7.50	0.00
$S_0 \rightarrow S_2$	$0.50\cdot(\pi_x \rightarrow \pi_y^*) + 0.50\cdot(\pi_y \rightarrow \pi_x^*)$	6.31	0.00
$S_0 \rightarrow S_1$	$0.50\cdot(\pi_x \rightarrow \pi_y^*) - 0.50\cdot(\pi_y \rightarrow \pi_x^*)$	6.08	0.00

Table S2. $\pi \rightarrow \pi^*$ transitions of *R*-1,3-dimethylallene

Transition	Configuration	E (eV)	Oscillator strength
$S_0 \rightarrow S_4$	$0.50\cdot(\pi_M \rightarrow \pi_M^*) - 0.46\cdot(\pi_P \rightarrow \pi_P^*)$	7.74	1.25
$S_0 \rightarrow S_3$	$0.49\cdot(\pi_P \rightarrow \pi_M^*) - 0.49\cdot(\pi_M \rightarrow \pi_P^*)$	7.27	$0.3 \cdot 10^{-3}$
$S_0 \rightarrow S_2$	$0.49\cdot(\pi_P \rightarrow \pi_M^*) + 0.49\cdot(\pi_M \rightarrow \pi_P^*)$	6.19	0.00
$S_0 \rightarrow S_1$	$0.49\cdot(\pi_M \rightarrow \pi_M^*) + 0.49\cdot(\pi_P \rightarrow \pi_P^*)$	5.96	0.00

Table S3. $\pi \rightarrow \pi^*$ transitions of spiropentadiene

Transition	Configuration	E (eV)	Oscillator strength
$S_0 \rightarrow S_4$	$0.67\cdot(\pi_y \rightarrow \pi_{x-y}^*) - 0.17\cdot(\pi_y \rightarrow \pi_{x+y}^*)$	6.15	$39.1 \cdot 10^{-3}$
$S_0 \rightarrow S_3$	$0.67\cdot(\pi_x \rightarrow \pi_{x-y}^*) + 0.17\cdot(\pi_x \rightarrow \pi_{x+y}^*)$	6.15	$39.1 \cdot 10^{-3}$
$S_0 \rightarrow S_2$	$0.57\cdot(\pi_y \rightarrow \pi_{x+y}^*) + 0.37\cdot(\pi_x \rightarrow \pi_{x+y}^*)$	4.91	$8.3 \cdot 10^{-3}$
$S_0 \rightarrow S_1$	$0.57\cdot(\pi_x \rightarrow \pi_{x+y}^*) - 0.37\cdot(\pi_y \rightarrow \pi_{x+y}^*)$	4.91	$8.3 \cdot 10^{-3}$

Table S4. $\pi \rightarrow \pi^*$ transitions of *S*-1,4-spiropentadiene

Transition	Configuration	E (eV)	Oscillator strength
$S_0 \rightarrow S_4$	$0.67\cdot(\pi_P \rightarrow \pi_{x-y}^*) + 0.18\cdot(\pi_M \rightarrow \pi_{x+y}^*)$	6.12	$67.6 \cdot 10^{-3}$
$S_0 \rightarrow S_3$	$0.67\cdot(\pi_M \rightarrow \pi_{x-y}^*) + 0.18\cdot(\pi_P \rightarrow \pi_{x+y}^*)$	6.12	$70.7 \cdot 10^{-3}$
$S_0 \rightarrow S_2$	$0.67\cdot(\pi_P \rightarrow \pi_{x+y}^*) - 0.18\cdot(\pi_M \rightarrow \pi_{x-y}^*)$	5.02	$11.9 \cdot 10^{-3}$
$S_0 \rightarrow S_1$	$0.67\cdot(\pi_M \rightarrow \pi_{x+y}^*) - 0.18\cdot(\pi_P \rightarrow \pi_{x-y}^*)$	5.02	$12.0 \cdot 10^{-3}$

TD-DFT may not be able to account for molecules where the electronic states have multireference character. We assess the multireference character of dimethylallene, dimethylspiropentadiene, and dimethylspirononatetraene by computing the D_1 and D_2 diagnostics of the ground state and the T_1 and T_2 diagnostics of the excited states. This is done by a CC2 computation using the def2-TZVP basis set as implemented in the Turbomole RICC2 code.[11-12] In the Turbomole code the T_1 and T_2 diagnostics are defined as a percentage, and we refer to the Turbomole manual for the specific definition.

The results are listed in Table S5, S6 and S7. For all three molecules the diagnostics indicate low or moderate multireference character in the singlet electronic states.

Table S5. CC2 results for *R*-1,3-dimethylallene.

State	E (eV)	D_1 / T_1	D_2 / T_2
S_4	8.96	92.3%	7.7%
S_3	8.15	93.2%	6.8%
S_2	7.40	93.0%	7.0%
S_1	6.47	93.7%	6.3%
S_0	0.00	0.032	0.146

Table S6. CC2 results for *S*-1,4-dimethylspiropentadiene.

State	E (eV)	D_1 / T_1	D_2 / T_2
S_4	6.44	92.5%	7.5%
S_3	6.43	92.5%	7.5%
S_2	5.23	91.9%	8.1%
S_1	5.23	91.9%	8.1%
S_0	0.00	0.032	0.145

Table S7. CC2 results for *S*-2,7-dimethylspirononatetraene.

State	E (eV)	D_1 / T_1	D_2 / T_2
S_4	6.08	90.3%	9.7%
S_3	6.08	90.4%	9.6%
S_2	4.76	90.3%	9.7%
S_1	4.75	90.4%	9.6%
S_0	0.00	0.043	0.162

To further test the findings using a multi-determinant wavefunction method, we use CASPT2 with cc-pVDZ basis set as implemented in the OpenMolcas 20.10 software suite.[13-14] State-averaged CASSCF is used to optimize the wavefunctions used for the CASPT2 computation. These computations were carried out primarily to verify how the excited states mix. The DFT-optimized structures were used for this purpose without further optimization. MOs are visualized using MOLDEN.[15]

Shown in Figure S1, an (8,8) active space was chosen for 1,3-dimethylallene covering the π-space and in part the σ-MOs relating to the methyl groups. In good qualitative agreement with the TD-DFT results, there is significant configuration interaction in the first four excited states, which involve excitation of orbitals of both helicities.

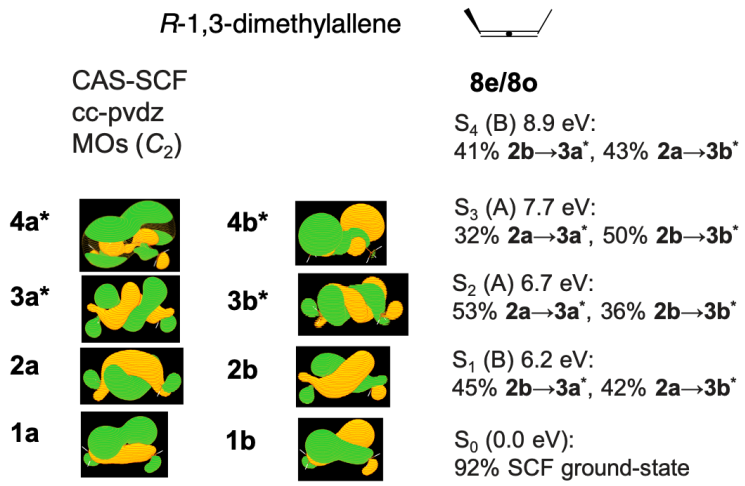

Figure S1. CASPT2 (8,8) computation of first four excited states of dimethylallene. Configurations contributing less than 4% are not listed.

Shown in Figure S2, we compare (4,4), (8,8), and (12,12) active spaces for 1,4-dimethylspiropentadiene. The (4,4) space covers the only the frontier π-MOs. The (8,8) space further covers the π-like σ-MOs on the central spiro-carbon. Finally, the (12,12) further includes σ-MOs which have their weight on the double-bonds and in part on the spiro-carbon. All three spaces provide good qualitative agreement with the TD-DFT results. In accordance with the symmetry restrictions, there is only interaction between configuration of same total symmetry. Consequently, the first four excited states do not involve near-degenerate orbitals of both helicities, only minor contributions of higher/lower energy excitations. The order of the A and B symmetry S_3 and S_4 change order upon moving into the (12,12) space, which is in accordance with the results using TD-DFT.

Shown in Figure S3, we further compare the effect of basis sets using the (12,12) active space for 1,4-dimethylspiropentadiene. Both 6-31(d,p) and def2-TZVP provide qualitative similar results to the cc-pvdz basis set, and to that using TD-DFT. The absolute energies of the transitions change, and quite notable the near-degenerate A and B symmetry S_1 and S_2 states are ordered differently when computed with def2-TZVP basis set.

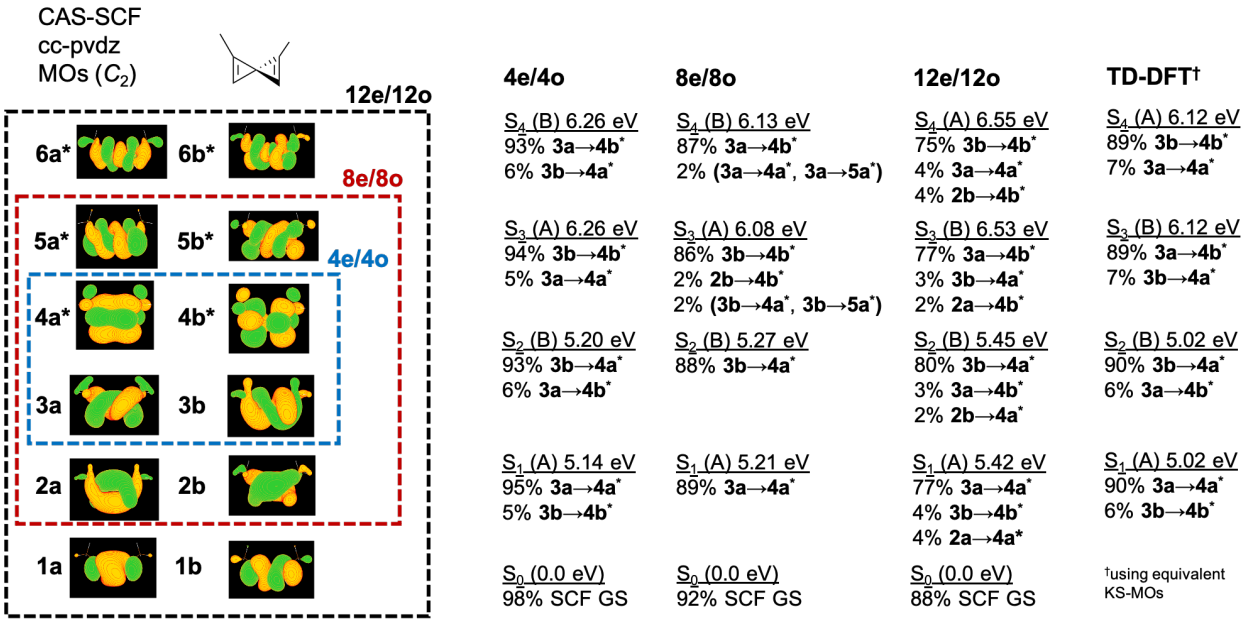

Figure S2. CASPT2 (4,4), (8,8) and (12,12) computations of first four excited states of dimethylspiropentadiene. Compared with TD-DFT ωB97X-D/def2-TZVP results. CAS-SCF MOs shown are optimized in the 12/12 active space but are visually identical when optimized in the two smaller active spaces. Configurations contributing less than 2% are not listed.

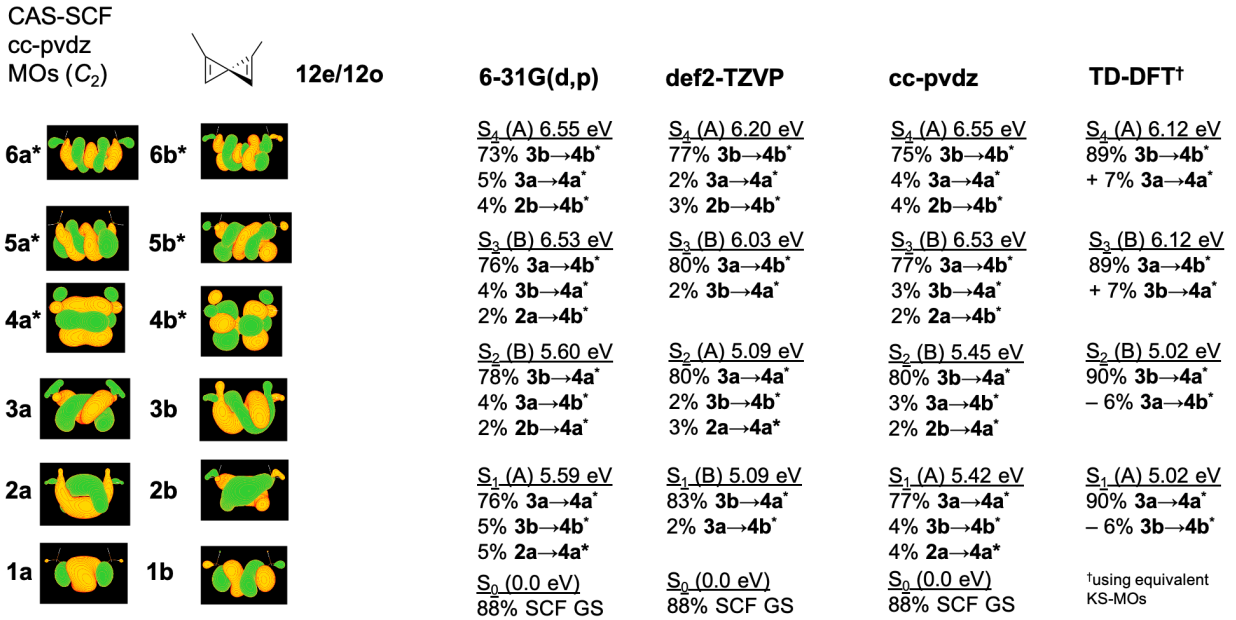

Figure S3. CASPT2(12,12) computations of first four excited states of dimethylspiropentadiene using 6-31G(d,p), def2-TZVP, and cc-pvdz basis sets. Compared with TD-DFT ωB97X-D/def2-TZVP results. CAS-SCF MOs shown are optimized in the 12/12 active space using cc-pvdz basis set but are visually very similar using the other basis sets. Configurations contributing less than 2% are not listed.

Shown in Figure S4, an (8,8) active space was chosen for 2,7-dimethylnonatetraene covering the π-space. Similar to dimethylspiropentadiene, there is good qualitative agreement with the TD-DFT results and the symmetry restrictions, there is only interaction between configuration of same symmetry. There is only minor configuration interaction from higher/lower energy excited states, which contribute few percent to the first four excited states.

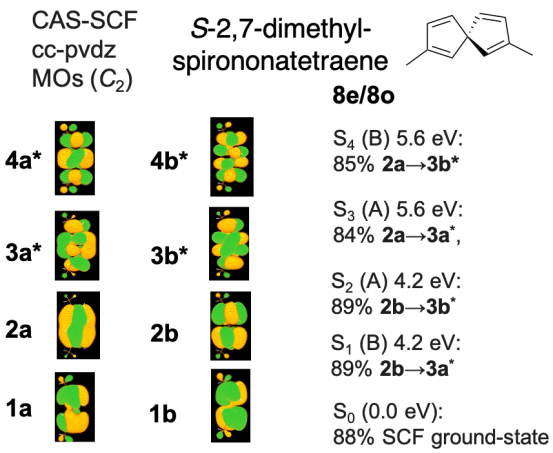

Figure S4. CASPT2 (8,8) computation of first four excited states of dimethylspirononatetraene. Configurations contributing less than 4% are not listed.

B. Schematic Overview of Change of Density

We are interested in understanding the patterns of $\Delta\rho$ which is appears in ab initio computations. To provide a simple assessment, we schematically draw up each type of occupied MO (π_x, π_y, π_M, π_P) and unoccupied MO (π_x^*, π_y^*, π_M^*, π_P^*) of allene and spiropentadiene. Naively, we can predict the change of electron based on a simple MO excitation by subtracting their squares (eq. S1). A superposition of two such MO excitations is the sum of this change.

$$\Delta\rho = |\pi^*|^2 - |\pi|^2 \qquad \text{(S1)}$$

$$\text{superposition } \Delta\rho = \Delta\rho_1 + \Delta\rho_2 \qquad \text{(S2)}$$

In Figure S5, this assessment is carried out for allene and spiropentadiene. As one may expect, any single excitation from a linear to higher energy linear MO yields a linear change of density. A superposition of two such excitations will also be linear. Moving on to excitations between helical MOs, excitations from a helical to a higher energy helical MO gives a helical change if both MOs have same helicity; if they have opposite helicity there will be a helical sense of direction without forming a continuous helical pattern (a broken helix). A superposition of helical excitations will return to a linear change of density because certain regions have opposing change of density. In spiropentadiene, the excitations are from an occupied linear or helical π-MO into an unoccupied linear MO. The four different helical excitations yield the expected helical change of density. A superposition of the helical excitations returns the linear pattern; however, this is forbidden by symmetry in the actual molecules. Thus, all four excitations of substituted spiropentadiene yield a helical change of density, as we see using TD-DFT computations presented in the manuscript.

It is also apparent that for the superposition $\Delta\rho$ the density change is the same for all four transitions. This happens because the sign of the excited-state mixing disappears when the wavefunction is squared to obtain a density. It is also trivial to show that a superposition of helical-to-helical excitations yields the same linear change of density as the superposition of linear-to-linear transitions. The helical MOs themselves are a superposition of two linear MOs (eq. S3).[16]

$$\pi_P = \pi_y + \pi_x,\ \pi_M = \pi_y - \pi_x \qquad \text{(S3)}$$

Now take a superposition of two such transitions into helical unoccupied MOs and insert the helical MOs expressed by linear MOs.

superposition $\Delta\rho = |\pi_y^* + \pi_x^*|^2 - |\pi_y + \pi_x|^2 + |\pi_y^* - \pi_x^*|^2 - |\pi_y - \pi_x|^2$ (S4)

By expanding the squares and simplifying, eq. S5 is reached, which following renormalization is simply the superposition of two linear transitions.

$\Delta\rho = |\pi_y^*|^2 + |\pi_x^*|^2 + 2\,|\pi_y^*|\cdot|\pi_x^*| - |\pi_y|^2 - |\pi_x|^2 - 2|\pi_y|\cdot|\pi_x| + |\pi_y^*|^2 + \pi_x^*|^2 - 2|\pi_y^*|\cdot|\pi_x^*| - |\pi_y|^2 - |\pi_x|^2 + 2|\pi_y|\cdot|\pi_x|$

$= 2\,(\,|\pi_y^*|^2 - |\pi_y|^2 + |\pi_x^*|^2 - |\pi_x|^2\,)$ (S5)

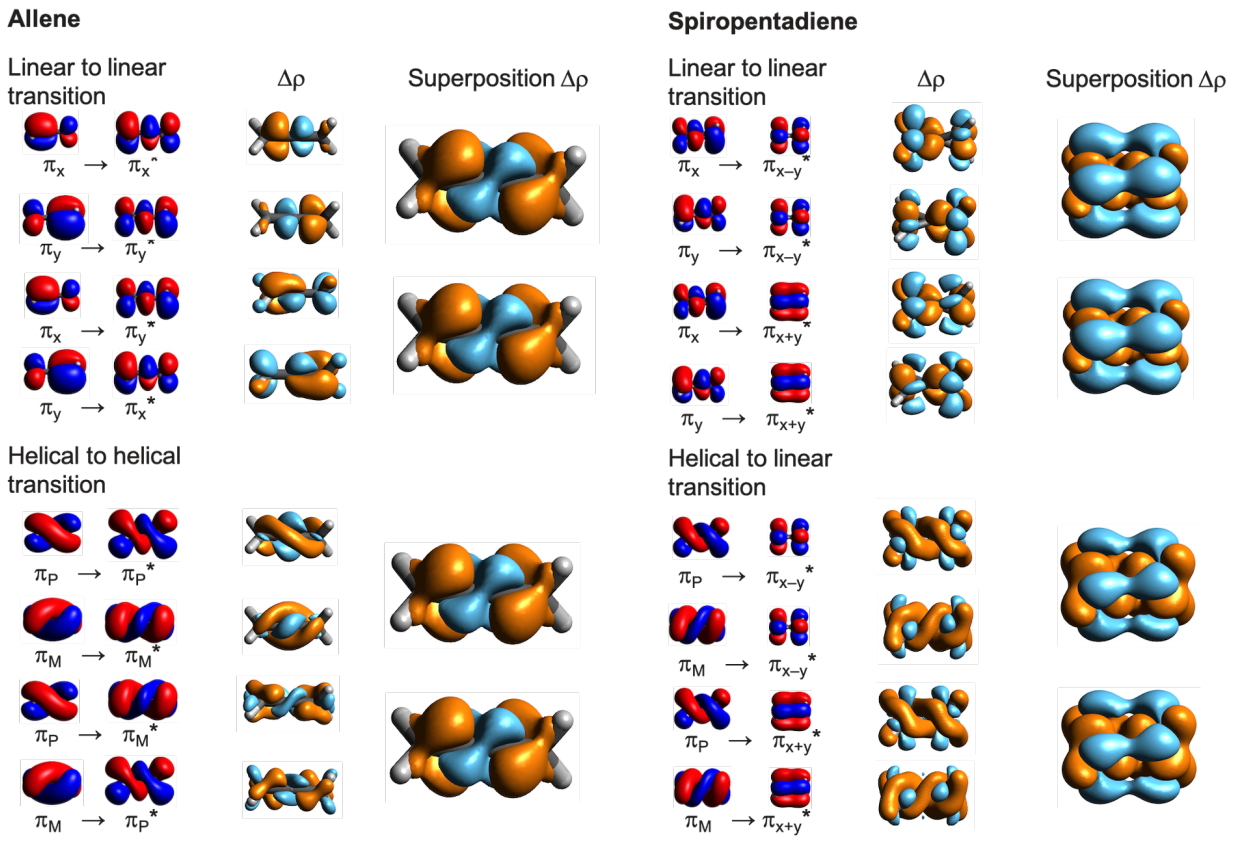

Figure S5. Schematic overview of the density change in allene and spiropentadiene. The MOs of unsubstituted allene and spiropentadiene are squared and subtracted using equation S1 and S2. Depletion of density is shown in orange.

C. Cyclically-linked Molecules

Due to the structural similarity to cyclohexane, 1,3-butadiylallene assumes a chair and a twist-boat conformation. These are shown in Figure S6 along with the frontier MOs. The twist conformer is found to be slightly more stable than the chair by 33 meV.

The helical MOs are significantly changed compared to dimethylallene and consequently the electronic transitions change in 1,3-butadiylallene. Shown in the simulated ECD spectrum in Figure S6b, multiple transitions give rise to optical activity. We speculate this is related to the changed MO contributions to the electronic transitions (figure S6c). The change of electron density is helical in $S_0 \rightarrow S_2$, and $S_0 \rightarrow S_3$, with opposite sign depending on the helicity. $S_0 \rightarrow S_4$ is not a $\pi \rightarrow \pi^*$ transition as other close-lying MOs mix into the transition.

1,3-butadiylspiropentadiene has same two conformations as the butadiylallene; however, only chair conformer is most relevant as it is 55 meV lower energy than the twist conformer. For completeness, we include both conformers in the overview in Figure S7. The helical HOMO and HOMO-1 are energetically split in 1,3-butadiylspiropentadiene and consequently the electronic transitions change. As the electronic transitions are energetically split, the rotatory strength gives rise to big $\Delta\varepsilon$ in the simulated ECD spectrum in Figure S7b. The helicity of the electronic transition is almost lost in the change of density in cases where the MO excitations mix almost equally.

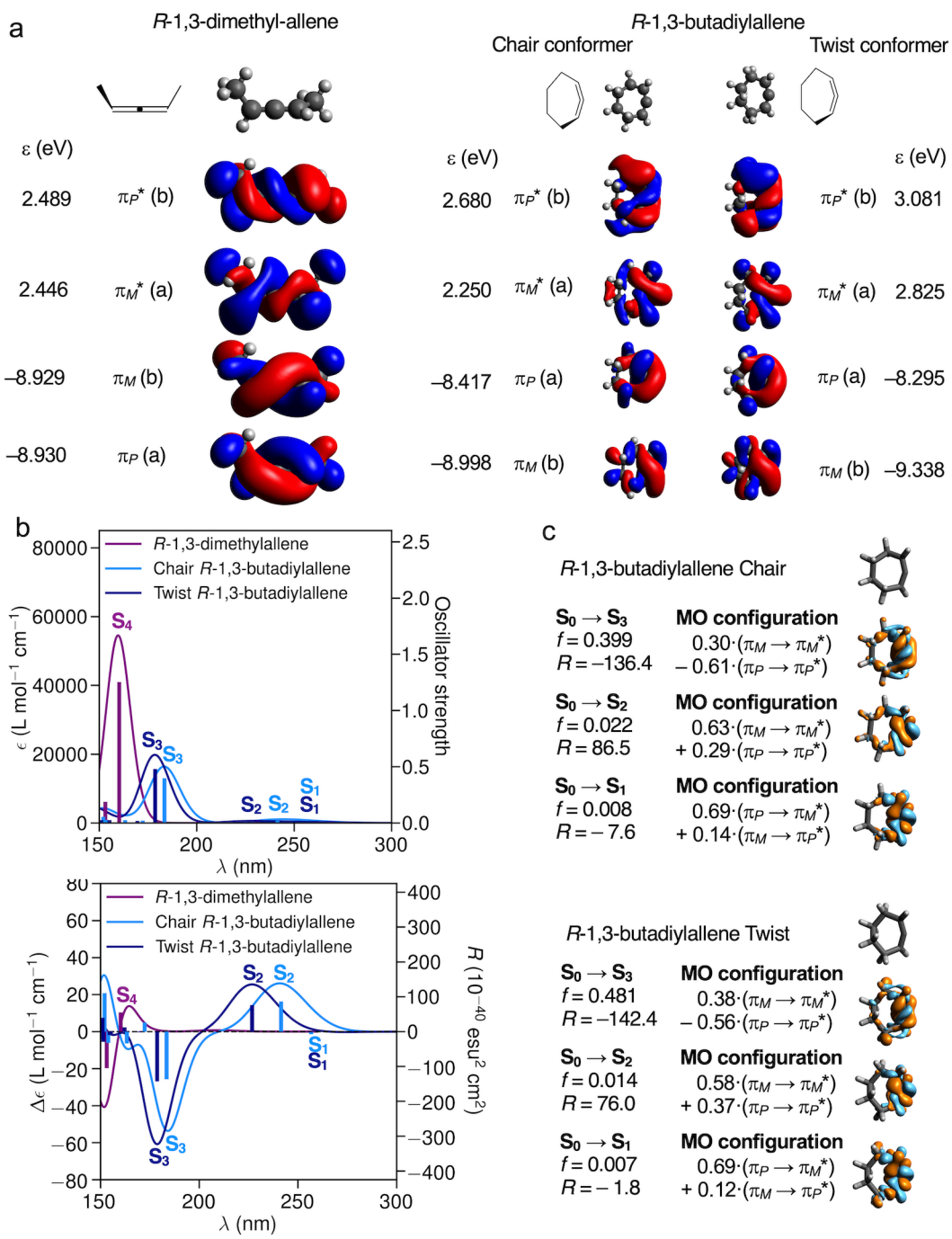

Figure S6. a) Frontier MOs of 1,3-dimethylallene and cyclically linked 1,3-butadiylallene. b) Simulated UV-Vis and ECD. Transitions are marked by their final state. c) Change of electron density of *R*-1,3-butadiylallene for the $S_0 \rightarrow S_1$, $S_0 \rightarrow S_2$, and $S_0 \rightarrow S_3$ electronic transitions computed at the ωB97X-D/def2-TZVP level.[1-2] Oscillator strengths, *f*, are dimensionless. Rotatory strengths, *R*, are in 10^{40} erg·esu·cm/Gauss. Depletion of density is in orange. Iso-value = 0.002.

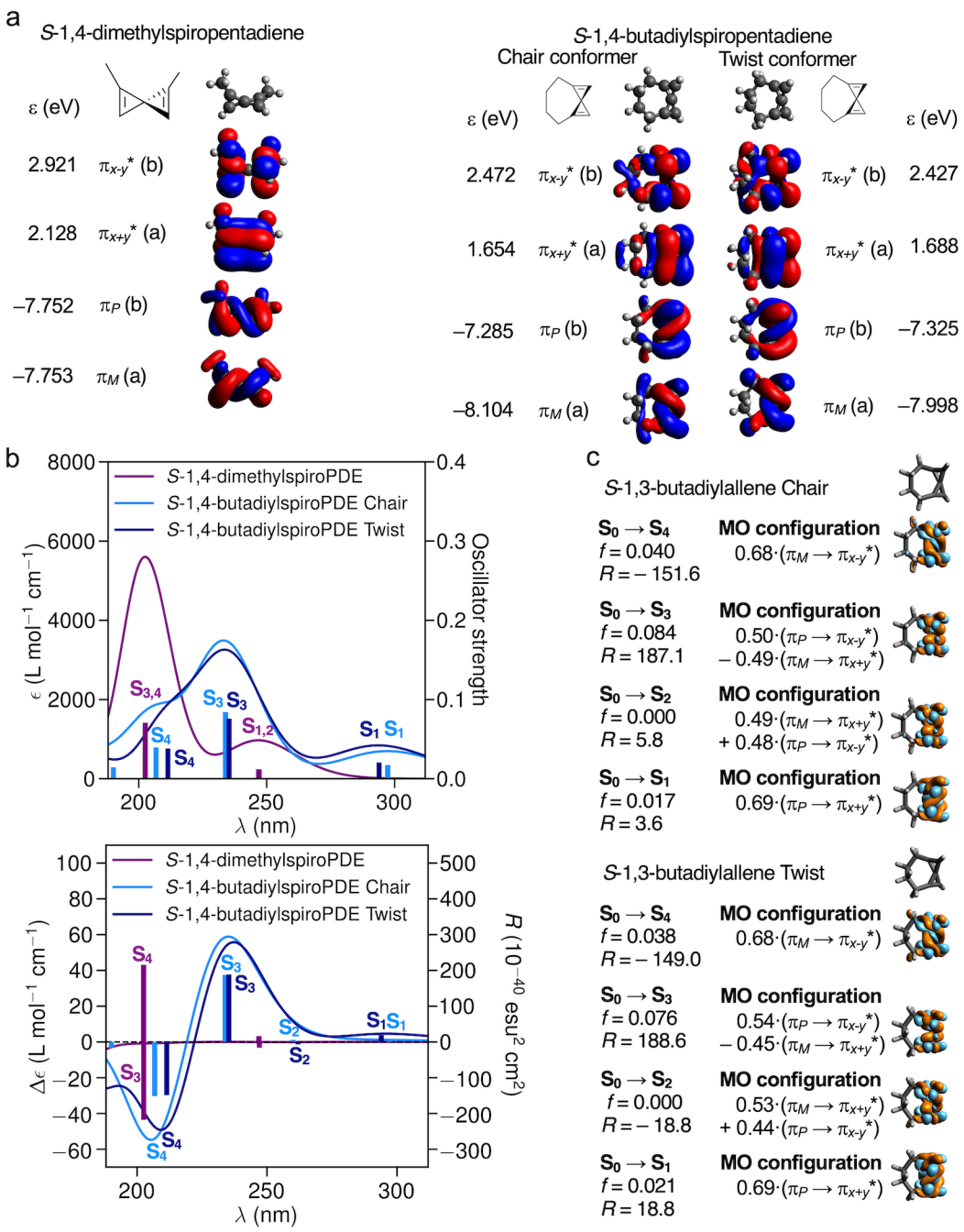

Figure S7. a) Frontier MOs of 1,4-dimethylspiropentadiene and cyclically-linked 1,4-butadiylspiropentadiene b) Simulated UV-Vis and ECD spectra. Transitions are marked by their final state. c) Change of electron density of *S*-1,4-butadiylspiropentadiene for the $S_0 \rightarrow S_1$, $S_0 \rightarrow S_2$, $S_0 \rightarrow S_3$ and $S_0 \rightarrow S_4$ electronic transitions computed at the ωB97X-D/def2-TZVP level.[1-2] Oscillator strengths, *f*, are dimensionless. Rotatory strengths, *R*, are in 10^{40} erg·esu·cm/Gauss. Depletion of density is in orange. Iso-value = 0.002.

D. Silicon and Germanium analogues

The silicon and germanium analogues of spiropentadiene have similar molecule structure to the carbon system, and the same symmetry arguments apply. For simplicity we have chosen to use the same substituents as in the carbon system, although larger substituents are typically used synthetically to improve the kinetic stability of the compounds.

The main difference between spiropentadiene and its sila- and germa-analogues, is that there are σ-MOs that are close to the HOMO-LUMO gap, which mix significantly into the π-π* transitions. Furthermore, the helical π-MOs have less weight on the central spiro-carbon.

Listed in Figure S8b, the transitions helicity is to some extend preserved in $S_0 \rightarrow S_1$ and $S_0 \rightarrow S_2$, but is largely lost in $S_0 \rightarrow S_3$ and $S_0 \rightarrow S_4$ where multiple MO excitations contribute. It is clear that the electronic transitions can be helical in substituted spiropentasiladienes and spiropentagermadienes, but they are more liable to mixing of excitations involving σ-MOs. This may also depend on the choice of substituents.

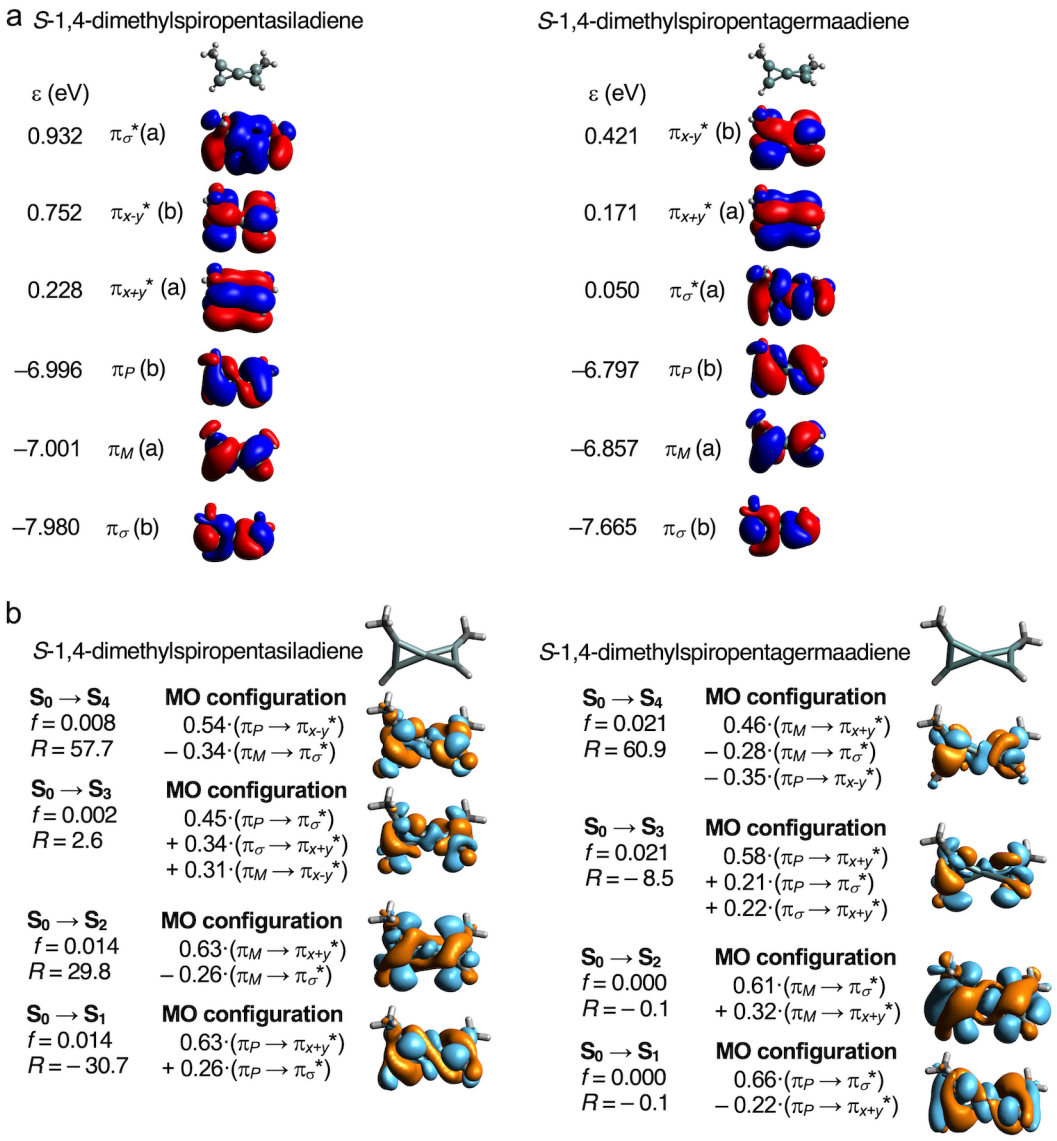

Figure S8. HOMO-1 to LUMO+3 of dimethylspiropentasiladiene and dimethylspiropentagermadiene computed at the ωB97X-D/def2-TZVP level.[1-2] The MOs are shown with an the Iso-value = 0.01. b) Overview of $S_0 \rightarrow S_1$ to $S_0 \rightarrow S_4$ electronic transitions and their symmetry designations, and computed change of electron. Oscillator strengths, *f*, are dimensionless. Rotatory strengths, *R*, are in 10^{40}erg·esu·cm/ Gauss). Depletion of density is in orange. Iso-value = 0.001.

E. Spirononatetraene

Like spiropentadiene and allene, spirononatetraene has D_{2d} symmetry.[17-18] While its electronic structure is similar to spiropentadiene, spirononatetraene has four more π-electrons and therefore the MO symmetries switch. Thus the HOMO-2 and HOMO-3 (π_x and π_y), and the LUMO and LUMO+1 (π_x and π_y) are degenerate, while the HOMO and HOMO-1 (π_{x+y} and π_{x-y}) are non-degenerate and delocalize via through-space overlap, as shown in Figure S8. Upon disubstitution the HOMO-2 and HOMO-3 (π_P and π_M) mix and show clear helicity. The LUMO and LUMO+1 (π_P* and π_M*) also become helical, which can be seen by close inspection of the nodal planes (there are none between the two π-systems). However, their much sharper twist means the helicity is less obvious. The HOMO-2 and HOMO-3 (π_P and π_M) are clearly helical, but will be less relevant for observable properties. An overview of the electronic transitions are provided in Figure S9. Most of the helicity is lost in the transitions due to the weak helicity in (π_P* and π_M*).

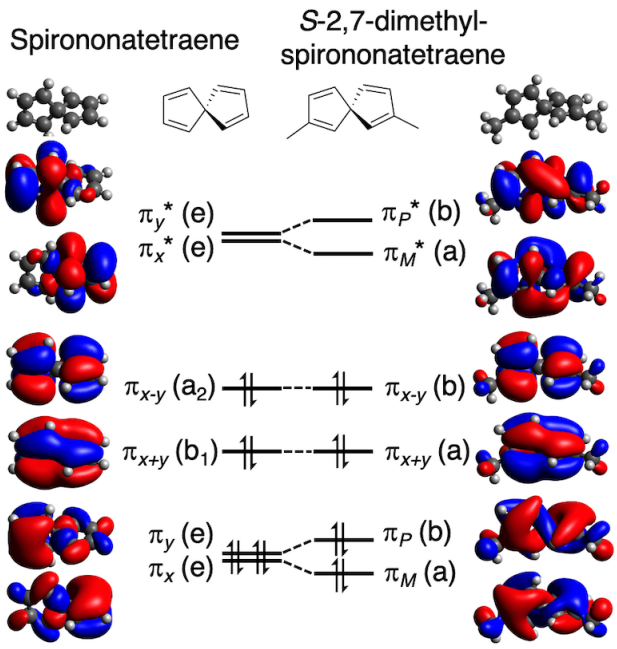

Figure S9. HOMO-3 to LUMO+1 of spirononatetraene and *S*-2,7-dimethylspirononatetraene computed at the ωB97X-D/def2-TZVP level.[1-2]

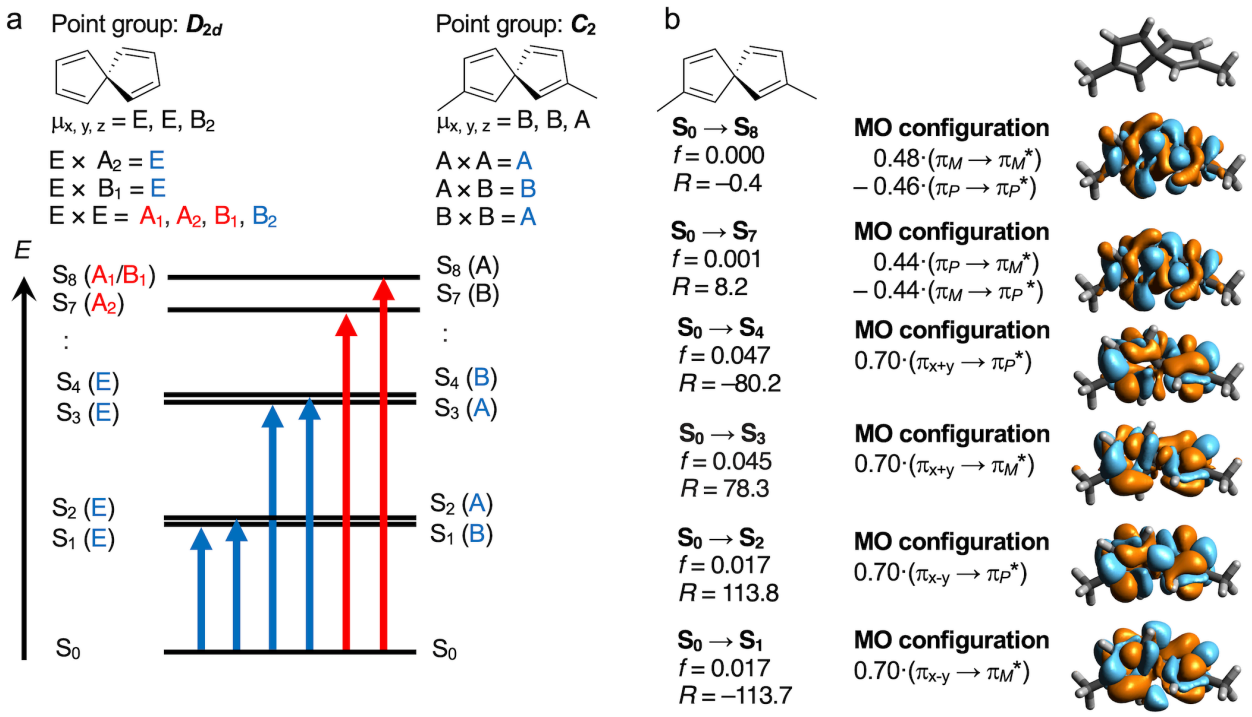

Figure S10. a) Overview of $S_0 \rightarrow S_1$ through $S_0 \rightarrow S_4$, and $S_0 \rightarrow S_7$ and $S_0 \rightarrow S_8$ electronic transitions of spirononatetraene and *S*-2,7-dimethylspirononatetraene, and their symmetry designations. Electric-dipole allowed transitions are marked in blue. b) Change of electron density for the $S_0 \rightarrow S_1$ through $S_0 \rightarrow S_4$, and $S_0 \rightarrow S_7$ and $S_0 \rightarrow S_8$ electronic transitions of *S*-2,7-dimethylspirononatetraene. Oscillator strengths, *f*, are dimensionless. Rotatory strengths, *R*, are in 10^{40} erg·esu·cm/ Gauss). Depletion of density is in orange. Iso-value = 0.001.

F. Tricyclic Spiro-analogues

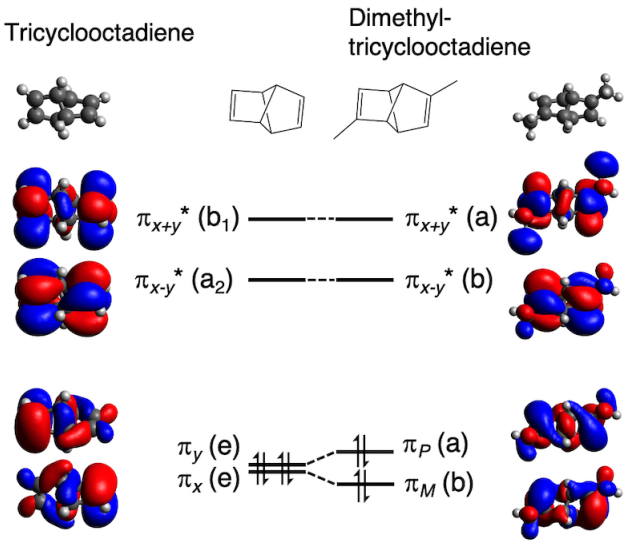

Figure S11. HOMO-1 to LUMO+1 of spiro-analogues tricyclooctadiene and dimethyltricyclooctadiene computed at the ωB97X-D/def2-TZVP level.[1-2]

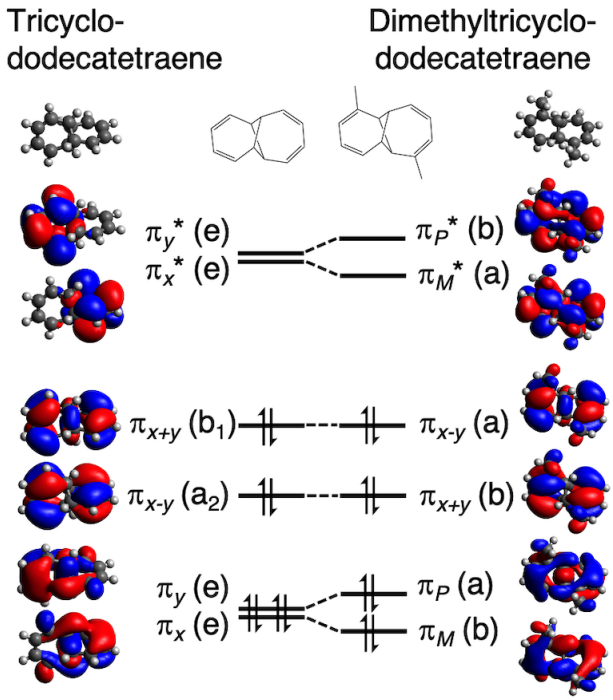

Figure S12. HOMO-3 to LUMO+1 of spiro-analogues tricyclododecatetraene and dimethyl tricyclododecatetraene computed at the ωB97X-D/def2-TZVP level.[1-2]

REFERENCES

1. Chai, J.-D.; Head-Gordon, M. Long-Range Corrected Hybrid Density Functionals with Damped Atom–Atom Dispersion Corrections. *Phys. Chem. Chem. Phys.* **2008**, *10*, 6615-6620.
2. Weigend, F.; Ahlrichs, R. Balanced Basis Sets of Split Valence, Triple Zeta Valence and Quadruple Zeta Valence Quality for H to Rn: Design and Assessment of Accuracy. *Phys. Chem. Chem. Phys.* **2005**, *7*, 3297-3305.
3. M. J. Frisch, G. W. T., H. B. Schlegel, G. E. Scuseria, M. A. Robb, J. R. Cheeseman, G. Scalmani, V. Barone, G. A. Petersson, H. Nakatsuji, X. Li, M. Caricato, A. V. Marenich, J. Bloino, B. G. Janesko, R. Gomperts, B. Mennucci, H. P. Hratchian, J. V. Ortiz, A. F. Izmaylov, J. L. Sonnenberg, D. Williams-Young, F. Ding, F. Lipparini, F. Egidi, J. Goings, B. Peng, A. Petrone, T. Henderson, D. Ranasinghe, V. G. Zakrzewski, J. Gao, N. Rega, G. Zheng, W. Liang, M. Hada, M. Ehara, K. Toyota, R. Fukuda, J. Hasegawa, M. Ishida, T. Nakajima, Y. Honda, O. Kitao, H. Nakai, T. Vreven, K. Throssell, J. A. Montgomery, Jr., J. E. Peralta, F. Ogliaro, M. J. Bearpark, J. J. Heyd, E. N. Brothers, K. N. Kudin, V. N. Staroverov, T. A. Keith, R. Kobayashi, J. Normand, K. Raghavachari, A. P. Rendell, J. C. Burant, S. S. Iyengar, J. Tomasi, M. Cossi, J. M. Millam, M. Klene, C. Adamo, R. Cammi, J. W. Ochterski, R. L. Martin, K. Morokuma, O. Farkas, J. B. Foresman, and D. J. Fox *Gaussian 16, Revision A.03*, Gaussian, Inc., Wallingford CT: 2016.
4. Hanwell, M. D.; Curtis, D. E.; Lonie, D. C.; Vandermeersch, T.; Zurek, E.; Hutchison, G. R. Avogadro: An Advanced Semantic Chemical Editor, Visualization, and Analysis Platform. *Journal of Cheminformatics* **2012**, *4*, 17.
5. http://avogadro.cc/ *Avogadro: An Open-Source Molecular Builder and Visualizationtool. Version 1.2.0*, 2020.
6. Bode, B. M.; Gordon, M. S. Macmolplt: A Graphical User Interface for Gamess. *Journal of Molecular Graphics and Modelling* **1998**, *16*, 133-138.
7. Mardirossian, N.; Head-Gordon, M. Thirty Years of Density Functional Theory in Computational Chemistry: An Overview and Extensive Assessment of 200 Density Functionals. *Molecular Physics* **2017**, *115*, 2315-2372.
8. Autschbach, J. Computing Chiroptical Properties with First-Principles Theoretical Methods: Background and Illustrative Examples. *Chirality* **2009**, *21*, E116-E152.
9. Srebro-Hooper, M.; Autschbach, J. Calculating Natural Optical Activity of Molecules from First Principles. *Annu. Rev. Phys. Chem.* **2017**, *68*, 399-420.
10. Dennington, R.; Keith, T. A.; Millam, J. M. *Gaussview, Version 6.1*, Semichem Inc., Shawnee Mission, KS: 2016.
11. Balasubramani, S. G.; Chen, G. P.; Coriani, S.; Diedenhofen, M.; Frank, M. S.; Franzke, Y. J.; Furche, F.; Grotjahn, R.; Harding, M. E.; Hättig, C., et al. Turbomole: Modular Program Suite for Ab Initio Quantum-Chemical and Condensed-Matter Simulations. *J. Chem. Phys.* **2020**, *152*, 184107.
12. *Turbomole V7.1, 2016, Forschungszentrum Karlsruhe Gmbh, 1989-2007, Turbomole Gmbh, since 2007*.
13. Fdez. Galván, I.; Vacher, M.; Alavi, A.; Angeli, C.; Aquilante, F.; Autschbach, J.; Bao, J. J.; Bokarev, S. I.; Bogdanov, N. A.; Carlson, R. K., et al. Openmolcas: From Source Code to Insight. *J. Chem. Theory Comput.* **2019**, *15*, 5925-5964.

14. Aquilante, F.; Autschbach, J.; Baiardi, A.; Battaglia, S.; Borin, V. A.; Chibotaru, L. F.; Conti, I.; De Vico, L.; Delcey, M.; Fdez. Galván, I., et al. Modern Quantum Chemistry with [Open]Molcas. *J. Chem. Phys.* **2020**, *152*, 214117.
15. Schaftenaar, G.; Noordik, J. H. Molden: A Pre- and Post-Processing Program for Molecular and Electronic Structures*. *J. Comput. Aided Mol. Des.* **2000**, *14*, 123-134.
16. Garner, M. H.; Hoffmann, R.; Rettrup, S.; Solomon, G. C. Coarctate and Möbius: The Helical Orbitals of Allene and Other Cumulenes. *ACS Cent. Sci.* **2018**, *4*, 688-700.
17. Haselbach, E.; Allan, M.; Bally, T.; Bednarek, P.; Sergenton, A.-C.; de Meijere, A.; Kozhushkov, S.; Piacenza, M.; Grimme, S. Spiro[4.4]Nonatetraene and Its Positive and Negative Radical Ions: Molectronic Structure Investigations. *Helv. Chim. Acta* **2001**, *84*, 1670-1693.
18. Sowa, J. K.; Mol, J. A.; Briggs, G. A. D.; Gauger, E. M. Spiro-Conjugated Molecular Junctions: Between Jahn–Teller Distortion and Destructive Quantum Interference. *J. Phys. Chem. Lett.* **2018**, *9*, 1859-1865.